Parametric mapping of vector basis functions for surface integral equation formulations

Andrew F. Peterson and Keith R. Aberegg
School of Electrical and Computer Engineering
Georgia Institute of Technology
Atlanta, GA 30332-0250
peterson@ee.gatech.edu

Abstract: A parametric mapping of vector basis functions is presented for curved-patch discretizations of surface integral equations. The mapping of the vector basis function maintains the normal continuity of the surface current density at cell boundaries, and is therefore suitable for use with the electric-field integral equation. Expressions for the matrix elements associated with the electric and magnetic field integral equations are developed.

1. Introduction

During the past two decades, the approximate solution of surface integral equations by the method of moments has matured into a well-accepted process. However, the most widely-used procedures tend to employ flat-cell models of curved structures and relatively low-order basis functions to represent surface currents and fields. Specifically, the Rao-Wilton-Glisson (RWG) triangular-rooftop basis functions [1] commonly used to model currents on surfaces in 3D provide only a constant normal and linear tangential representation of the surface current density. If higher accuracy in the results is desired, a low-order representation is likely to prove inefficient. Furthermore, flat cells limit the modeling resolution. In this article, we discuss the use of a higher-order vector basis set with continuity properties similar to the RWG functions, in conjunction with a curved-cell scatterer model.

The incorporation of curved cells into moment-method discretizations, although uncommon, has been discussed by a number of authors [2-8]. However, a critical issue in the discretization of surface integral equations such as the electric-field equation (EFIE) is the need to maintain continuity of the normal surface current density at cell junctions [1]. The existing literature on curved-cell representations fails to adequately address this issue. References [2] and [3] assumed a piecewise-constant representation for the current density, while [4] investigated both piecewise-constant and piecewise-linear representations. Thus, these studies did not always impose normal continuity because of the nature of the basis functions. In addition, [2] and [4] only consider the magnetic field integral equation (MFIE), which is less sensitive to discontinuities in the current density. References [5] and [6] employed mixed-order vector basis functions on curved triangular and quadrilateral cells, respectively, and a similar approach has been reported in [7]. These articles consider the use of low-order basis functions similar to the RWG functions and do not specifically discuss the continuity properties of the curved-cell representation.

Higher-order scalar polynomial basis functions have been investigated by numerous researchers in the context of finite element solutions [9-10]. Higher-order vector functions are less well known, but have also been studied [11-13]. In general, if the scatterer model incorporates curvature, there is little additional effort required to implement higher-order basis functions (other than the additional unknowns for a given number of cells, which may be offset by improved accuracy).

In this paper, we briefly review the scalar transformation required to treat the EFIE and MFIE applied to two-dimensional scatterers. We then consider the mapping necessary to define curved-cell vector basis functions compatible with 3D surface integral equations. The development is based on a cell-by-cell coordinate mapping obtained via Lagrangian interpolation polynomials. Other specific representations of the surface (e.g., splines) could be implemented in a similar manner. For illustration, we present preliminary results for a curved-cell implementation using vector basis functions one polynomial order greater than the RWG functions.

2. Discretization of 2D surface integral equations using an isoparametric quadratic representation

To motivate the use of higher-order basis functions and curved-cell models, this section briefly reviews their application in 2D. Two-dimensional method-of-moments discretization schemes employing flat-cell models of the scatterer contours and piecewise-constant or piecewise-linear basis functions have been widely used [14]. The scatterer models can be improved by using cells with parabolic curvature. Suppose t is a parametric variable with the interval $-1 \le t \le 1$ used to describe a single cell. The cell can be defined by the three points (x_1,y_1), (x_2,y_2), and (x_3,y_3), and the mapping

$$x(t) = x_1 B_1(t) + x_2 B_2(t) + x_3 B_3(t) \qquad (1)$$

$$y(t) = y_1 B_1(t) + y_2 B_2(t) + y_3 B_3(t) \qquad (2)$$

where

$$B_1(t) = \frac{t(t-1)}{2} \qquad (3)$$

$$B_2(t) = 1 - t^2 \qquad (4)$$

$$B_3(t) = \frac{t(t+1)}{2} \qquad (5)$$

are quadratic Lagrangian interpolation functions. It is convenient to also use quadratic Lagrangian interpolation polynomials to represent the surface current density, which is known as an isoparametric expansion. For a smooth scatterer, and the TM polarization, the current density within a cell can be replaced by

$$J_z(t) \equiv \sum_{n=1}^{3} j_n B_n(t) \qquad -1 \le t \le 1 \qquad (6)$$

Thus, within each cell there are three overlapping basis functions that contribute to the representation. Each basis function interpolates to the current density at one of the three "nodes" that define the cell shape, according to (1)–(2).

Consider the TM EFIE, and the use of Dirac delta testing functions (located at the interpolation nodes) to complete the discretization. The entries of the system matrix involve integrals of the form

$$I_{mn}^{\text{cell p}} = \frac{k\eta}{4} \int_{\text{cell p}} B_n(t') H_0^{(2)}(kR_m) J(t') dt' \qquad (7)$$

where m and n now denote global indices,

$$R_m = \sqrt{[x_m - x(t')]^2 + [y_m - y(t')]^2} \qquad (8)$$

and J is the Jacobian

$$J(t) = \sqrt{\left(\frac{dx}{dt}\right)^2 + \left(\frac{dy}{dt}\right)^2} \qquad (9)$$

The Jacobian can be evaluated using the mapping in (1)–(2), which yields

$$\frac{dx}{dt} = \left(\frac{x_3 - x_1}{2}\right) + (x_1 - 2x_2 + x_3)\, t \qquad (10)$$

$$\frac{dy}{dt} = \left(\frac{y_3 - y_1}{2}\right) + (y_1 - 2y_2 + y_3)\, t \qquad (11)$$

within a particular cell. In general, the integrals defined by (7) must be evaluated by numerical quadrature. In the case where R_m vanishes within the interval of integration, the Hankel function singularity can be extracted, splitting the integral into two parts. The first integral can be computed by quadrature; the second can be evaluated analytically over a flat cell. As an alternative approach, the original integral can be evaluated using a quadrature rule that specifically incorporates the logarithmic singularity [15-16].

For the TE MFIE, a similar discretization can be developed, using an expansion similar to (6) for the transverse component of the current. The off-diagonal matrix entries involve integrals of the form

$$I_{mn}^{\text{cell p}} = \frac{k}{4j} \int_{\text{cell p}} B_n(t') \left\{ \sin\Omega(t') \frac{x_m - x(t')}{R_m} - \cos\Omega(t') \frac{y_m - y(t')}{R_m} \right\} H_1^{(2)}(kR_m) J(t') dt' \qquad (12)$$

where the Jacobian J is defined in (9), R_m is defined in (8), and Ω denotes the continuous angle between the x-axis and the tangent vector to each point on the cell. If node m lies at an intercell node, the diagonal matrix entries for the MFIE have the form

$$Z_{mm} = -\frac{\Gamma_m}{2\pi} + I_{mm}^{\text{cell p}} + I_{mm}^{\text{cell q}} \qquad (13)$$

where Γ_m denotes the total interior wedge angle formed by the conductor at node m, and $I_{mm}^{\text{cell p}}$ and $I_{mm}^{\text{cell q}}$ have the form of (12), except that a small region in the vicinity of node m is excluded from the integral. (The integral was

evaluated using an "open" quadrature formula that did not sample at the endpoints of the interval; a region on the order of 10^{-5} λ is easily excluded by this procedure.) If node m lies in the cell interior, the MFIE diagonal entries are

$$Z_{mm} = -\frac{1}{2} + I_{mm}^{cell\ p} \qquad (14)$$

where again a small region around node m is excluded from the integral.

To illustrate the accuracy of the isoparametric Lagrangian approach, Table 1 shows the TE surface current density induced on a circular cylinder by a uniform plane wave. Results from a curved-cell discretization of the MFIE using piecewise-quadratic basis functions are compared to similar solutions obtained using a flat-cell discretization with piecewise-constant and piecewise-linear representations of the current density. For a density of 40 unknowns/λ, there is a consistent improvement in accuracy as the basis function order is increased. The curved-cell results exhibit four decimal places of agreement with the exact solution.

In general, numerical experimentation using a range of cell sizes tends to confirm that the error in the 2D surface current density follows the predicted interpolation error of $O(h^{p+1})$ as $h \to 0$, where h is the relative cell size and p is the polynomial degree of the basis functions (p=2 denotes quadratic functions, for instance). Thus, it is more efficient to obtain high accuracy by increasing the polynomial order than by reducing the cell sizes. Additional results using this type of mapping with a combined-field formulation are presented in [17].

Table 1

Comparison of the current density induced on a circular cylinder with circumference 1 λ by a TE plane wave propagating in the ϕ=0 direction. MFIE results obtained with pulse, linear, and quadratic basis functions and Dirac delta testing functions are compared with the exact solution, for a 40 unknown discretization. The quadratic case employs parabolic cells defined by (1)–(2); the other results were obtained using flat cells.

ϕ	MFIE pulse basis, flat cells	MFIE linear basis, flat cells	MFIE quadratic basis, parabolic cells	exact
		(magnitude)		
0°	0.8907	0.8891	0.8883	0.8882
45	0.6733	0.6729	0.6722	0.6722
90	1.1751	1.1708	1.1714	1.1713
135	1.6232	1.6201	1.6199	1.6199
180	1.7094	1.7076	1.7073	1.7071
		(phase)		
0°	66.29°	66.66°	66.56°	66.56°
45	113.41	113.57	113.56	113.56
90	-164.88	-164.80	-164.82	-164.82
135	-125.83	-125.82	-125.84	-125.84
180	-110.77	-110.82	-110.83	-110.83

3. Mapping vector basis functions to curvilinear cells in 3D

The previous section showed that higher-order basis functions and curved cells can produce improved accuracy in scalar problems. The process of mapping scalar basis functions to curved cells in two and three dimensions is explained in a number of textbooks [9-10], and is widely understood. A transformation defined by a small number of points (nodes) on the curved cell uniquely specifies the mapped functions. Neighboring cells can be defined by independent mappings that share nodes along the common edges. Usually, the continuity of the scalar basis functions is maintained across curved cell boundaries, although derivative continuity is not. (Derivative continuity can be maintained by alternative mappings involving spline functions or Hermitian interpolation polynomials.)

One would expect to realize a similar improvement in accuracy from the use of higher-order functions and curved cells in vector problems, such as the 3D EFIE. When transforming vector basis functions, however, there is an additional degree of freedom embodied in the vector direction of the function that was not present in the scalar case. Thus, the vector mapping process is somewhat different from that used with scalar basis functions. A local mapping that describes the curved cell shape via Lagrangian polynomials will generally not be able to maintain the complete continuity of a vector basis function across cell boundaries. For the treatment of surface integral equations such as the EFIE, the surface current density must maintain normal continuity across cell junctions, in order that the surface divergence of the current remains finite at the cell edges. Therefore, it is critical to define the vector projection in a way that ensures normal continuity. In addition, to treat surface integral equations the mapping involves a two-dimensional surface in three-dimensional space. Crowley has discussed the mapping of a tangentially-continuous vector representation (the complementary case), for application to the vector Helmholtz equation [18]. A covariant mapping preserves tangential continuity. Apparently, no detailed discussion of the appropriate parametric mapping needed for surface integral equations exists at present in the electromagnetics literature. Normal continuity can be preserved by using a contravariant mapping, as described below.

For illustration, the following development considers a curved quadrilateral cell shape; the same expressions apply to triangular cells provided that the limits of integration are modified accordingly. Consider a basis function defined in the 2D reference cell ($-1<\eta<1$, $-1<\xi<1$). This vector can be represented by its covariant components

$$\bar{B} = (\bar{B}\cdot\bar{\eta})\,\bar{\eta}' + (\bar{B}\cdot\bar{\xi})\,\bar{\xi}' \tag{15}$$

or its contravariant components

$$\bar{B} = (\bar{B}\cdot\bar{\eta}')\,\bar{\eta} + (\bar{B}\cdot\bar{\xi}')\,\bar{\xi} \tag{16}$$

where the base vectors are given by

$$\bar{\eta} = \frac{\partial x}{\partial \eta}\hat{x} + \frac{\partial y}{\partial \eta}\hat{y} + \frac{\partial z}{\partial \eta}\hat{z} \tag{17}$$

$$\bar{\xi} = \frac{\partial x}{\partial \xi}\hat{x} + \frac{\partial y}{\partial \xi}\hat{y} + \frac{\partial z}{\partial \xi}\hat{z} \tag{18}$$

and the reciprocal base vectors are given by

$$\bar{\eta}' = \frac{\partial \eta}{\partial x}\hat{x} + \frac{\partial \eta}{\partial y}\hat{y} + \frac{\partial \eta}{\partial z}\hat{z} \tag{19}$$

$$\bar{\xi}' = \frac{\partial \xi}{\partial x}\hat{x} + \frac{\partial \xi}{\partial y}\hat{y} + \frac{\partial \xi}{\partial z}\hat{z} \tag{20}$$

In a skewed quadrilateral cell, the base vectors are tangential to the cell edges while the reciprocal base vectors are normal to the cell edges. The mapping from the 2D reference cell to the curved patch in 3D can be defined by a transformation of the form

$$x = \sum_n x_n B_n(\eta,\xi) \tag{21}$$

$$y = \sum_n y_n B_n(\eta,\xi) \tag{22}$$

$$z = \sum_n z_n B_n(\eta,\xi) \tag{23}$$

where $\{B_n\}$ represents a set of scalar Lagrangian interpolation functions (of any order), and the nodes (x_n,y_n) specify the specific patch shape. Therefore, the Jacobian relationship is given by

$$\begin{bmatrix} \frac{\partial}{\partial \eta} \\ \frac{\partial}{\partial \xi} \end{bmatrix} = \begin{bmatrix} \frac{\partial x}{\partial \eta} & \frac{\partial y}{\partial \eta} & \frac{\partial z}{\partial \eta} \\ \frac{\partial x}{\partial \xi} & \frac{\partial y}{\partial \xi} & \frac{\partial z}{\partial \xi} \end{bmatrix} \begin{bmatrix} \frac{\partial}{\partial x} \\ \frac{\partial}{\partial y} \\ \frac{\partial}{\partial z} \end{bmatrix} = \mathbf{J} \begin{bmatrix} \frac{\partial}{\partial x} \\ \frac{\partial}{\partial y} \\ \frac{\partial}{\partial z} \end{bmatrix} \tag{24}$$

For use with surface integral equations, the basis functions must be tangential to the curved patch at every point within the patch, and ensure normal continuity between adjacent patches. These characteristics can be obtained if the

Cartesian components of the basis function in each cell are defined by the contravariant mapping

$$\begin{bmatrix} B_x \\ B_y \\ B_z \end{bmatrix} = \frac{1}{Q} \mathbf{J}^T \begin{bmatrix} B_\eta \\ B_\xi \end{bmatrix} \tag{25}$$

where B_η and B_ξ denote the contravariant components of the basis function in the reference cell,

$$Q = \sqrt{\left(\frac{\partial y}{\partial \eta}\frac{\partial z}{\partial \xi} - \frac{\partial z}{\partial \eta}\frac{\partial y}{\partial \xi}\right)^2 + \left(\frac{\partial z}{\partial \eta}\frac{\partial x}{\partial \xi} - \frac{\partial x}{\partial \eta}\frac{\partial z}{\partial \xi}\right)^2 + \left(\frac{\partial x}{\partial \eta}\frac{\partial y}{\partial \xi} - \frac{\partial y}{\partial \eta}\frac{\partial x}{\partial \xi}\right)^2} \tag{26}$$

is the pseudo-determinant of the 2×3 Jacobian matrix, and we assume that the basis functions B_η and B_ξ maintain normal continuity in the reference cell. The factor Q defines the scaling necessary to write the differential surface area

$$dS = Q\, d\eta d\xi \tag{27}$$

in terms of the (η, ξ) coordinates.

When working with mapped basis functions, it is convenient to perform the calculations directly in the (η,ξ) system. Thus, we would like to express the integrals arising from the EFIE in terms of η and ξ. For a basis function defined by Equation (25), it is possible to show that the surface divergence operation on a curved cell simplifies to

$$\nabla_s \cdot \bar{B} = \frac{1}{Q}\left\{\frac{\partial B_\eta}{\partial \eta} + \frac{\partial B_\xi}{\partial \xi}\right\} \tag{28}$$

By combining Equations (27) and (28), the contribution from one cell to the scalar potential integral within the EFIE can be written as

$$\Phi = \frac{1}{j\omega\varepsilon}\int\int (\nabla_s' \cdot \bar{B}_n)\, G\, dS' =$$

$$\frac{1}{j\omega\varepsilon}\int_{\eta'=-1}^{1}\int_{\xi'=-1}^{1}\left\{\frac{\partial B_\eta}{\partial \eta'} + \frac{\partial B_\xi}{\partial \xi'}\right\} G\, d\eta' d\xi' \tag{29}$$

where G denotes the Green's function. Since the testing functions are also defined by the transformation in (25), a general form for the complete matrix entry is

$$\int\int \bar{T}_m \cdot \nabla\Phi\, dS$$

$$= -\int\int (\nabla \cdot \bar{T}_m)\, \Phi\, dS$$

$$= -\int_{\eta=-1}^{1}\int_{\xi=-1}^{1}\left\{\frac{\partial T_{m\eta}}{\partial \eta} + \frac{\partial T_{m\xi}}{\partial \xi}\right\} \Phi\, d\eta d\xi \tag{30}$$

Using (25) and (27), the matrix entry associated with the magnetic vector potential term in the EFIE can be written in terms of the integral

$$\int\int \bar{T}_m(\bar{r}) \cdot \left\{\int\int \bar{B}_n(\bar{r}')\, G\, dS'\right\} dS$$

$$= \int_{\eta=-1}^{1}\int_{\xi=-1}^{1}\int_{\eta'=-1}^{1}\int_{\xi'=-1}^{1}\left[T_{m\eta}\ T_{m\xi}\right] \mathbf{J}\,\mathbf{J}^T \begin{bmatrix} B_{n\eta} \\ B_{n\xi} \end{bmatrix} G\, d\eta' d\xi' d\eta d\xi \tag{31}$$

Thus, in these integrals the scale factors arising from the basis and testing functions cancel those arising from the differential surface areas. The matrix entries associated with the MFIE can also be expressed over curved patches; for instance the off-diagonal entries have the form

$$\int\int \bar{T} \cdot \bar{H}^s\, dS =$$

$$\int_\eta\int_\xi\int_{\eta'}\int_{\xi'} \left[T_\eta\ T_\xi\right] \mathbf{J} \begin{bmatrix} 0 & -\frac{\partial G}{\partial z} & \frac{\partial G}{\partial y} \\ \frac{\partial G}{\partial z} & 0 & -\frac{\partial G}{\partial x} \\ -\frac{\partial G}{\partial y} & \frac{\partial G}{\partial x} & 0 \end{bmatrix} \mathbf{J}^T \begin{bmatrix} B_\eta \\ B_\xi \end{bmatrix} d\eta' d\xi' d\eta d\xi \tag{32}$$

while the diagonal entries differ in the usual way due to the total field term and the Green's function singularity.

The general expressions in (30)–(32) provide a convenient way of computing the matrix entries when a piecewise-parametric representation is used to define the curved surface. All integrals can be performed over the square reference cell in the (η, ξ) coordinate system by numerical quadrature. In the case of a triangular reference cell, the limits of integration in (30)–(32) must be modified to incorporate the triangular cell shape.

4. Higher-order vector basis functions for surface currents

The surface current representation proposed in 1982 by Rao, Wilton and Glisson [1] has a constant normal component and a linear tangential component (CN/LT) around the cell edges. Better accuracy could be obtained with higher-order polynomial functions. Functions have been proposed that provide a linear normal, quadratic-tangent (LN/QT) representation of the surface current density, and exhibit finite divergence throughout the computational domain [13]. As compared with an RWG representation, where three basis functions overlap each cell, eight different

LN/QT basis functions overlap each triangular cell. Six of these functions have support shared by two triangular cells, like the RWG CN/LT functions. Each of these six functions interpolates to the normal vector component of the surface current at one end of a cell edge. These six functions maintain normal-vector continuity with the adjoining cell, and eliminate fictitious charge densities at cell interfaces. Equivalently, the surface divergence of the representation remains finite. Within a single cell, these six edge-based basis functions can be expressed as

$$\hat{z} \times w_{ij} L_i \nabla L_j, \qquad i \neq j \tag{33}$$

where $\{L_1, L_2, L_3\}$ denote simplex coordinates [9-10] within a triangle in the x-y plane, and w_{ij} is the length of the edge between nodes i and j. (L_1 and L_2 play the role of the local coordinates η and ξ in the expressions from the preceding section, with L_3 defined by $L_3 = 1 - L_1 - L_2$.) In addition, there are two basis functions in each cell whose support is confined to that cell. These cell-based functions can be expressed in simplex coordinates as

$$\hat{z} \times 4w_{13}\{L_2 L_3 \nabla L_1 - L_1 L_2 \nabla L_3\} \tag{34}$$

and

$$\hat{z} \times 4w_{23}\{L_1 L_3 \nabla L_2 - L_1 L_2 \nabla L_3\} \tag{35}$$

These two functions have zero normal component along all three edges of the cell, and together provide a quadratic representation for the tangential component of the current density. The LN/QT basis functions have been motivated by the development of complementary techniques for discretizing the curl-curl form of the vector Helmholtz equation [19]. The basis functions belong to the mixed-order divergence-conforming spaces originally proposed by Nedelec [11], which include representations for arbitrary polynomial order. For a triangular-cell model, the global LN/QT representation consists of two basis functions per non-boundary edge and two basis functions per cell. Figure 1 depicts these basis functions.

The 8 basis functions in Equations (33)–(35) are linearly independent and can be used as testing functions within a Galerkin implementation, if desired. However, for simplicity we propose the use of piecewise-constant "razor-blade" testing functions defined along linearly independent paths that roughly correspond to the basis function locations, as depicted in Figure 2.

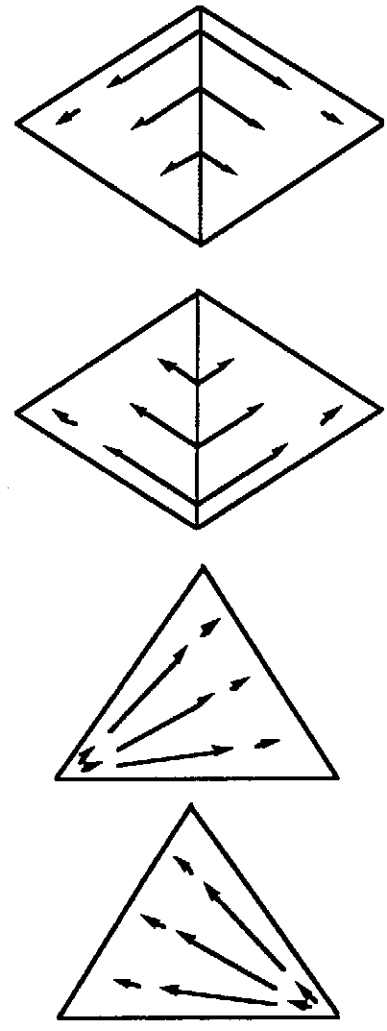

Figure 1. The linear-normal/quadratic-tangential (LN/QT) basis functions defined on a triangular cell. The upper two triangles depict the edge-based functions, while the lower two depict the cell-based functions.

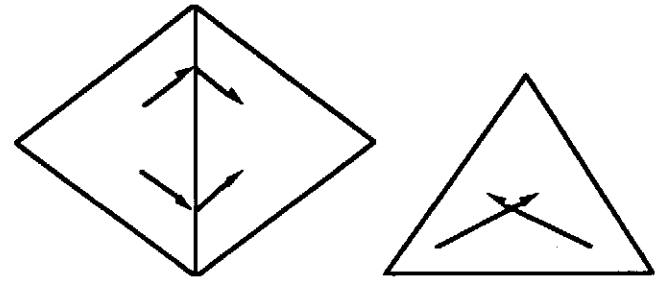

Figure 2. Domain of support for the razor-blade testing functions on triangles. The left cell shows the path for the edge-based functions; the right shows the path for the cell-based functions.

5. Preliminary results

To demonstrate the preceding ideas, we implemented the basis functions in (33)–(35) using a piecewise-parabolic surface representation defined by triangular-cell quadratic Lagrangian polynomials. Each patch is defined by the mapping in (21)–(23), using 6 scalar interpolation polynomials

$$B_{200}(L_1,L_2,L_3) = (2L_1 - 1)L_1 \quad (36)$$

$$B_{020}(L_1,L_2,L_3) = (2L_2 - 1)L_2 \quad (37)$$

$$B_{002}(L_1,L_2,L_3) = (2L_3 - 1)L_3 \quad (38)$$

$$B_{110}(L_1,L_2,L_3) = 4L_1L_2 \quad (39)$$

$$B_{101}(L_1,L_2,L_3) = 4L_1L_3 \quad (40)$$

$$B_{011}(L_1,L_2,L_3) = 4L_2L_3 \quad (41)$$

and 6 coordinate values at the corners and mid-sides of each cell. The first three functions have unity value at one corner node, while the latter three functions have unity value in the center of one of the three sides.

The functions in (36)–(41) define the shape of the curved cells comprising the scatterer, given six points per patch from which to interpolate according to (21)–(23). By converting from simplex coordinates to Cartesian coordinates [10], one readily obtains the entries of the Jacobian matrix defined in (24). The LN/QT basis functions defined in (33)–(35) are mapped to the curved cells using the contravariant projection in (25), and used to represent the vector surface current density. The matrix entries for the EFIE are obtained from (30)–(31), with the integration limits suitably modified for a triangular reference cell. Equations (30)–(31) account for the curved-cell mapping, so the only additional effort needed to implement the curved-cell discretization is the computation of the Jacobian matrix at points needed for the quadrature algorithm used to evaluate (30) and (31). Since the integration is performed in the reference cell, it is not necessary to explicitly define the basis functions within the curved patches.

The evaluation of the matrix entries by numerical quadrature is straightforward except when the source and observation regions overlap, due to the Green's function singularity. In this case, the 1/R singularity is extracted and evaluated analytically over a tangent plane, then added back to the result of the quadrature.

For illustration, consider a plane wave illuminating a perfectly conducting sphere of radius 0.2 λ, where λ denotes the wavelength. Figures 3a, 3b, 4a, and 4b depict the magnitude and phase of the surface currents around the sphere. The surface current density is normalized to the magnitude of the incident magnetic field. The incident field propagates in the –z direction with the electric field polarized in the –x direction. Exact solutions are compared to EFIE results obtained using curved-cell and flat-cell models, each of which consist of 48 cells and produce a moment-method system of order 240. Both results employed LN/QT basis functions and razor-blade testing functions. Clearly, the curved-cell data more closely approximates the exact solution. Since the basis functions provide normal continuity but not tangential continuity, there are a few places where jump discontinuities can be observed in these plots. These discontinuities occur in places where the tangential component contributes to the current density shown in the plot, and they diminish as the model is refined and the cell sizes are reduced. Figure 5 shows the scattering cross section comparison for the same example. In this case, the flat-cell model is inscribed within the actual sphere and the scattering cross section differs substantially from the true values.

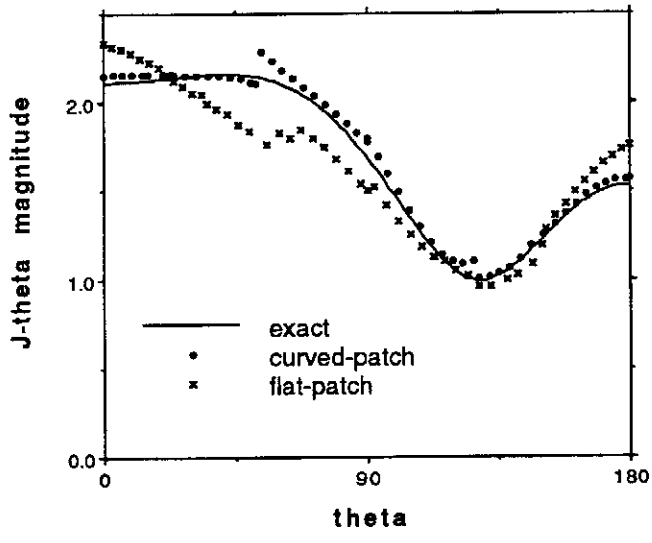

Figure 3(a). The magnitude of the θ-component of the current density induced by a uniform plane wave on a spherical conducting scatterer with radius 0.2 wavelengths. Numerical results produced using LN/QT basis functions with a flat-cell model and a curved-cell model are compared with the exact solutions. The models contained 48 cells and produced a system of order 240.

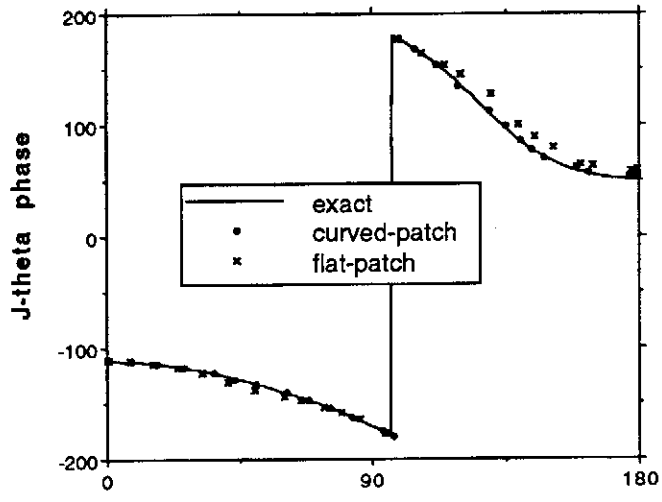

Figure 3(b). The phase of the θ-component of the current density for the example in Figure 3(a).

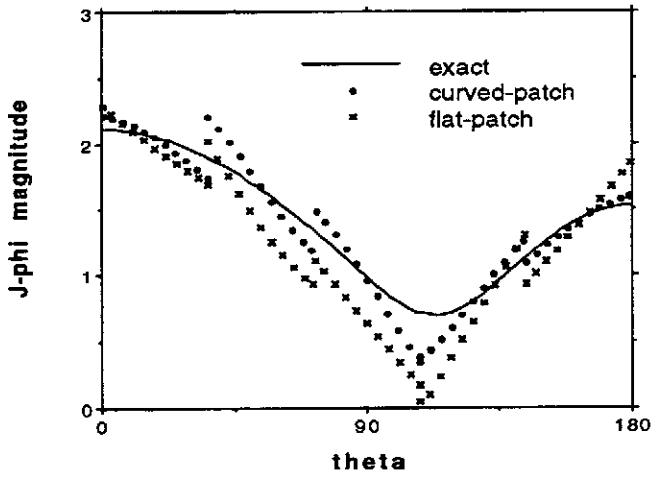

Figure 4(a). The magnitude of the ϕ-component of the current density for the example in Figure 3(a).

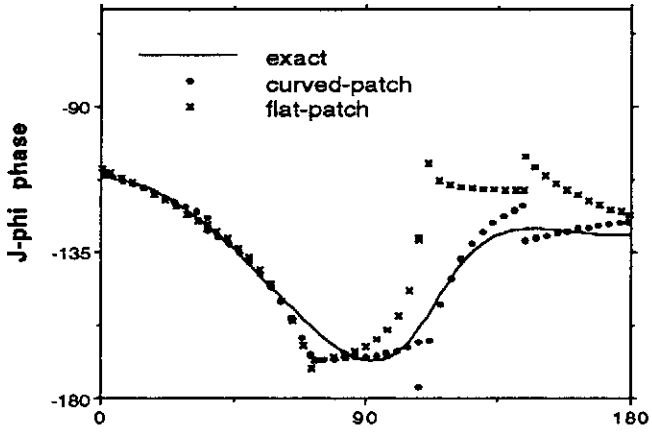

Figure 4(b). The phase of the ϕ-component of the current density for the example in Figure 3(a).

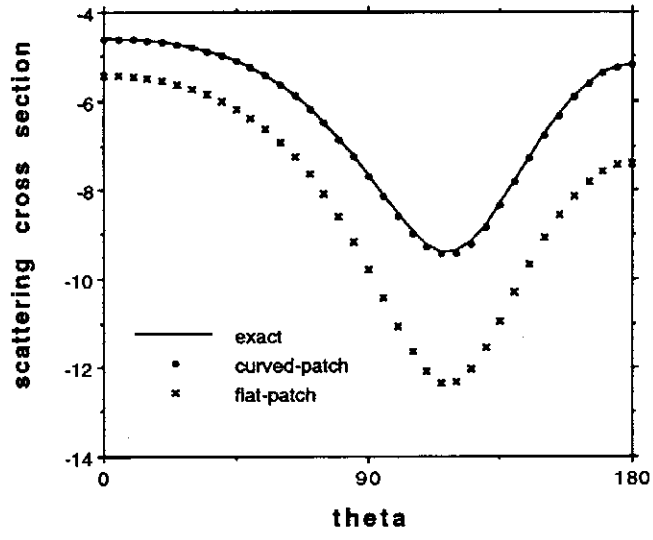

Figure 5. The scattering cross section (dB λ^2) for a spherical conducting scatterer with radius 0.2 wavelengths, shown for ϕ=0. Numerical results obtained using LN/QT basis functions with flat-cell and curved-cell models are compared with the exact solution. The models contained 48 cells and produced a system of order 240. The substantial difference in the accuracy of the numerical results may be due in part to the fact that the flat-cell model was inscribed within the desired sphere.

6. Summary

In practice, the accuracy of most numerical solutions is limited by the interpolation error associated with the expansion, and the use of higher-order functions and curved cells is expected to provide better accuracy and faster convergence. This paper presents a procedure for defining vector basis functions on curved cells, while maintaining the normal-vector continuity of the representation. Expressions for the matrix entries arising from EFIE and MFIE discretizations are presented. The 3D procedure has been implemented using LN/QT basis functions and curved triangular patches defined by a scalar Lagrangian mapping. Additional 3D results based on the EFIE, MFIE, and combined field equation are available in [20].

7. References

[1] S. M. Rao, D. R. Wilton, and A. W. Glisson, "Electromagnetic scattering by surfaces of arbitrary shape," *IEEE Trans. Antennas Propagat.*, vol. AP-30, pp. 409-418, May 1982.

[2] D. L. Knepp and J. Goldhirsh, "Numerical analysis of electromagnetic radiation properties of smooth conducting bodies of arbitrary shape," *IEEE Trans. Antennas Propagat.*, vol. AP-20, pp. 383-388, May 1972.

[3] M. I. Sancer, R. L. McClary, and K. J. Glover, "Electromagnetic computation using parametric geometry," *Electromagnetics*, vol. 10, pp. 85-103, 1990.

[4] M. S. Ingber and R. H. Ott, "An application of the boundary element method to the magnetic field integral equation," *IEEE Trans. Antennas Propagat.*, vol. 39, pp. 606-611, May 1991.

[5] N. Y. Zhu and F. M. Landstorfer, "Application of curved parametric triangular and quadrilateral edge elements in the moment method solution of the EFIE," *IEEE Microwave and Guided Wave Letters*, vol. 3, pp. 319-321, Sept. 1993.

[6] G. E. Antilla and N. G. Alexopoulos, "Scattering from complex three-dimensional geometries by a curvilinear hybrid finite element - integral equation approach," *J. Opt. Soc. Amer. A*, vol. 11, pp. 1445-1457, April 1994.

[7] D. Wilkes and C. C. Cha, "Method of moments solution with parametric curved triangular patches," *Digest of the 1991 IEEE Antennas and Propagation Society International Symposium*, London, ON, pp. 1512-1515, June 1991.

[8] J. M. Song and W. C. Chew, "Moment method solutions using parametric geometry," *J. Electromagnetic Waves Applics.*, vol. 9, pp. 73-81, 1995.

[9] O. C. Zienkiewicz and R. L. Taylor, *The Finite Element Method*. London: McGraw-Hill, 1988.

[10] P. P. Silvester and R. L. Ferrari, *Finite Elements for Electrical Engineers*. Cambridge: Cambridge University Press, 1990.

[11] J. C. Nedelec, "Mixed finite elements in R3," *Numer. Math.*, vol. 35, pp. 315-341, 1980.

[12] S. Wandzura, "Electric current basis functions for curved surfaces," *Electromagnetics*, vol. 12, pp. 77-91, 1992.

[13] A. F. Peterson, "Higher-order surface patch basis functions for EFIE formulations," *Digest of the 1994 IEEE Antennas and Propagation Society International Symposium*, Seattle, WA, pp. 2162-2165, June 1994.

[14] R. F. Harrington, *Field Computation by Moment Methods*. Macmillan, 1968.

[15] S. Wandzura, "Accuracy in computation of matrix elements of singular kernels," *Proceedings of the Eleventh Annual Review of Progress in Applied Computational Electromagnetics*, Monterey, CA, pp. 1170-1176, March 1995.

[16] J. Ma, V. Rokhlin, and S. Wandzura, "Generalized Gaussian quadrature rules for systems of arbitrary functions," Research Report YALEU/DCS/RR-990, Yale University, October 1993.

[17] K. R. Aberegg and A. F. Peterson, "Application of the integral equation – asymptotic phase method to two-dimensional scattering," *IEEE Trans. Antennas Propagat.*, vol. 43, pp. 534-537, May 1995.

[18] C. W. Crowley, *Mixed-order Covariant Projection Finite Elements for Vector Fields*. Ph.D. Dissertation, McGill University, Montreal, Quebec, 1988.

[19] A. F. Peterson, "Vector finite element formulation for scattering from two-dimensional heterogeneous bodies," *IEEE Trans. Antennas Propagat.*, vol. 43, pp. 357-365, March 1994.

[20] K. R. Aberegg, "Electromagnetic scattering using the integral equation - asymptotic phase method," Ph.D. dissertation, Georgia Institute of Technology, Atlanta, 1995.